Theory and simulation of classical and quantum echoes

G. Manfredi* and M. R. Feix
Mathématiques Appliquées et Physique Mathematique d'Orléans, Université d'Orléans, Bâtiment de Mathématiques, Boîte Postale 6759, 45067 Orléans Cedex 2, France
(Received 13 October 1995)

Echo phenomena occurring in various physical systems are investigated, and analytical results are checked against computer experiments. It is found that Coulomb self-consistent interactions reduce the amplitude of the echo. Proof is given of the possibility of refocusing an initially localized packet by periodically kicking the particles, and the relation between this behavior and chaotic diffusion is discussed. Quantum echoes are investigated via simulations of the Wigner equation in the case of an anharmonic oscillator. It is shown that quantum effects allow for the appearance of linear echoes. The reversibility properties of classical and quantum many-particle systems are discussed. [S1063-651X(96)09206-9]

PACS number(s): 03.20.+i, 03.65.−w, 52.35.−g

I. INTRODUCTION

Although microscopic physical laws are symmetric in time, and therefore reversible in principle, macroscopic systems generally display an irreversible behavior (see, for example, Lebowitz [1] and references therein). As pointed out by Lebowitz, two ingredients are necessary to observe irreversibility. The first one is the fantastically large number of degrees of freedom contained in a macroscopic system compared to a microscopic one. The second ingredient is related to the observer who, for practical reasons, can only measure macroscopic, averaged quantities, such as density, temperature or pressure. In this work, we make use of several microscopical physical models, all of which are time reversal invariant (except for one case), and show how ''apparent'' irreversibility can rise when the two conditions mentioned above are fulfilled. We call this irreversibility ''apparent'' because the detailed, microscopic description is still reversible in principle, and there is no loss of information during the evolution. However, this microscopic information is not easily accessible: for example, it may be contained in the highly intricate structure of the phase space distribution function. Thus, in practice, for an observer measuring macroscopic quantities, the system displays an effectively irreversible behavior.

If one reverses the velocities of all the particles contained in the physical system, the initial condition will be recovered exactly. This is of course due to the fact that the underlying dynamical laws are time reversal invariant. However, velocity reversal is a microscopic operation, very sensitive to any perturbation, which can be performed with utmost difficulty in laboratory experiments (and even in computer simulations, given the finite number of digits available). This kind of microscopic reversibility has indeed been observed in very refined spin echo experiments [2]. A more interesting situation arises when one can induce reversible behavior by means of a macroscopic operation, although such a reversibility will generally be imperfect. Since most practical operations carried out in laboratory experiments involve a large number of particles, macroscopic reversibility should be, in principle, more easily testable than microscopic velocity reversal. This is the case, for example, of plasma wave echoes, first discovered theoretically by O'Neil and Gould [3], and subsequently observed in the laboratory [4].

O'Neil and Gould work out a perturbative theory of plasma wave echoes, which, like most perturbative approaches, soon becomes complicated, and of difficult physical interpretation: one of the aims of our paper is to provide some explicit numerical solutions, which may help our intuition and give more insight into the analytical treatment. In particular, O'Neil and Gould show that the echo still appears when there is no electrostatic interaction between the particles of the plasma. However, the effect of the self-consistent field on the echo is not evident from their work: we investigate this point in detail by means of numerical simulations. These computer experiments are carried out with a Vlasov Eulerian code [5,6], which has proven to display a very low level of noise compared to particle-in-cell codes.

In a second group of simulations we neglect the self-consistent interaction between the particles, which therefore can travel freely and are only subjected to external fields. In this case, a different initial condition is used, in which all particles are spatially concentrated in a region of very small size compared to the total box. Some interesting phenomena then arise, and we show that it is possible to prevent phase space filamentation by periodically applying a sinusoidal pulse. For these simulations, the integration of particle trajectories is exact (apart from round-off errors), therefore we adopt a Lagrangian (particle) code instead of an Eulerian one.

The last part of the paper is devoted to the investigation of quantum echoes. The Wigner picture of quantum mechanics [7,8] constitutes a valuable model, since it is based on a phase space representation, similar to the classical one. A kinetic, Eulerian code, recently developed by Suh and coworkers [9,10] has proven to be an excellent numerical tool. Here, we investigate the effect of a nonzero Planck constant on the formation of a linear echo for noninteracting particles confined by a prescribed anharmonic potential.

*Present address: United Kingdom Atomic Energy Authority, Fusion, Culham, Abingdon, OX14 3DB, United Kingdom.

II. SIMULATION OF PLASMA WAVE ECHOES

The physical system under consideration is a one-dimensional, collisionless, electrostatic plasma, formed of mobile electrons and a homogeneous, motionless, neutralizing background. This system is described by the Vlasov-Poisson equations, which, in dimensionless variables, read as

$$\frac{\partial f}{\partial t}+v\frac{\partial f}{\partial x}+E\frac{\partial f}{\partial v}=0, \quad \frac{\partial E}{\partial x}=\int f\,dv-1. \tag{1}$$

Note that Eqs. (1) do not contain any manifestly irreversible term (such as, for example, the collision integral in the Boltzmann equation for gas dynamics). In Eqs. (1) space is measured in units of the Debye length $\lambda_D=(\epsilon_0 T/ne^2)^{1/2}$, and a time in units of the inverse of the plasma frequency $\omega_p=(ne^2/\epsilon_0 m)^{1/2}$. Here n is the plasma density, e and m are, respectively, the electron charge and mass, and the temperature T is measured in energy units. The Debye length and the inverse plasma frequency represent the typical space and time scales in a collisionless plasma. In particular, collective oscillations have a frequency close to ω_p, and, for small temperatures or large wavelengths, obey the following dispersion relation: $\omega^2=\omega_p^2+3V_{\rm th}^2k^2$, where $V_{\rm th}=(T/m)^{1/2}$ is the thermal velocity. One of the most interesting features of Eqs. (1), first realized by Landau, is that density modulations are exponentially damped, with a damping rate $\gamma_L(k)$, even if the system does not contain any form of ''truly'' irreversible, collisional dissipation [11]. This collisionless damping is essentially a phase mixing phenomenon. In our case, the initial state is spatially homogeneous, and Maxwellian in velocity space, with thermal velocity $V_{\rm th}=1$. At time $t=0$, we excite an external field in the plasma, of the form

$$E_1=\alpha_1\cos(k_1x)\,\delta(t). \tag{2}$$

This field induces a velocity modulation, and right after, a density modulation, which eventually decays by Landau damping. Note, however, that the distribution function $f(x,v,t)$ never loses memory of the initial pulse, although the spatial density does, and so does, of course, the electric field. This is reminiscent of the two ingredients for irreversibility: in fact (a) the number of degrees of freedom in the Vlasov representation is virtually infinite, and, (b) the density and the electric field are macroscopic, averaged quantities (unlike the distribution function). After the first wave has damped away, we launch a second wave, at time $t=\tau$:

$$E_2=\alpha_2\cos(k_2x)\,\delta(t-\tau). \tag{3}$$

The density modulation induced by this second pulse also decays away: however, after a time much longer than the inverse Landau damping rate of the first two pulses, a third wave appears (the echo) as a modulation of the density at the wave number $k_{\rm echo}=k_2-k_1$. The echo is due to a nonlinear interaction between the two pulses, and is essentially a phenomenon of beating between two waves.

Before turning to the numerical simulations, we show that the echo time can be obtained by a very simple argument. The first pulse (2) launches a wave with a phase $\phi_1=k_1x+k_1vt$; the second pulse (3) does the same with $\phi_2=k_2x+k_2v(t-\tau)$. Taking the phase difference $\phi_2-\phi_1$, and requiring it to be stationary with respect to v, one finds

$$\frac{\partial}{\partial v}(\phi_2-\phi_1)=(k_2-k_1)t-k_2\tau=0,$$

which gives the echo time

$$t_{\rm echo}=\frac{k_2}{k_2-k_1}\tau. \tag{4}$$

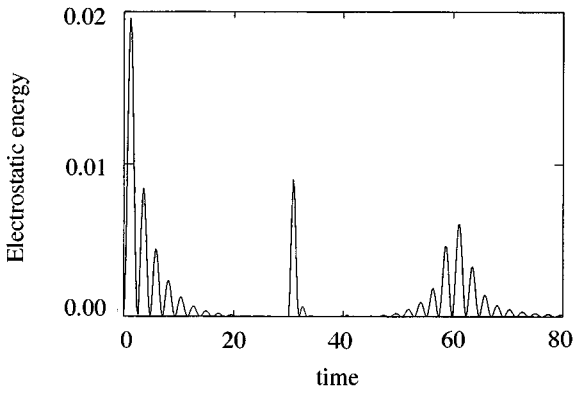

FIG. 1. Evolution of the electrostatic energy with time (expressed respectively in units of $mv_{\rm th}^2$ and ω_p^{-1}). The echo appears at $t=60\omega_p^{-1}$.

The numerical simulation of plasma echoes is a difficult problem, and examples of it do not abound in the literature [12,13]. In fact, the numerical method must be able to keep the information contained in the highly filamented distribution function until the time of the echo. In our simulations we make use of a kinetic, Eulerian code [5,6], which solves the Vlasov equation by direct discretization of the phase space. Such a code displays a very low noise level, even in zones of low density, and is thus to be preferred to usual particle-in-cell codes. As an example, we report the results of a simulation with the following physical parameters: $k_1\lambda_D=0.483$, $k_2\lambda_D=0.966$, $\omega_p\tau=30$, $\alpha_1=\alpha_2=0.1V_{\rm th}$. Note that, in our units, the α's represent the velocity modulation due to the pulses expressed in units of thermal velocity. Figure 1 shows the electrostatic energy as a function of time: the damping of the two pulses and the subsequent echo are accurately reproduced. The echo wave number is indeed k_2-k_1 as predicted by the theory. The Landau damping rate for the first pulse is $\gamma_L\simeq 0.4\omega_p$ [11], and even larger for the second pulse. The two pulses and the subsequent echo are thus well separated in time.

The plasma echo is chiefly a ballistic phenomenon and it is important to understand the effect of collective plasma oscillations on its appearance. In order to address this point, we perform a set of numerical simulations in which we let the Debye length vary. For noninteracting particles $\lambda_D=\infty$ and, by decreasing the value of λ_D, we switch on collective effects. However, both the thermal velocity and the total length of the plasma L are kept fixed, and since $\omega_p=\lambda_D^{-1}V_{\rm th}$, the plasma frequency also changes. Therefore, we no more measure time and space in unit of ω_p and λ_D,

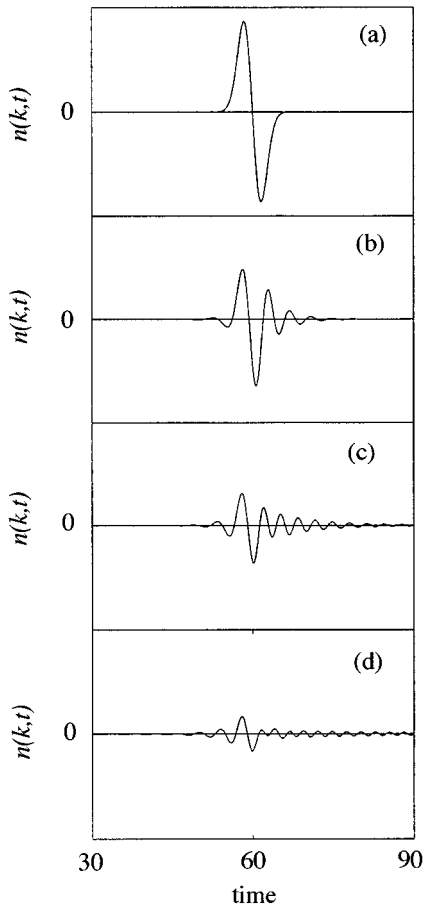

FIG. 2. Fourier component of the spatial density at wave number $k_{\rm echo}=k_2-k_1$ (arbitrary units for both axes). The normalized Debye length is $L\lambda_D^{-1}=0$ (a); $L\lambda_D^{-1}=0.1$ (b); $L\lambda_D^{-1}=0.15$ (c); and $L\lambda_D^{-1}=0.2$ (d).

but rather in ''ballistic'' units related to L for space, and $L/V_{\rm th}$ for time. Finally, the amplitude of the two pulses is rescaled in order to have the same velocity modulation; i.e., the α's are kept constant.

Although the previous description might seem complicated, we are just performing an experiment in which we progressively increase the particle charge q, while keeping all other parameters constant. Thus, the Debye length and the plasma frequency scale as $\lambda_D\propto q^{-1}, \omega_p\propto q$. We present a group of typical simulations for which we take $\alpha_1=\alpha_2=0.05V_{\rm th}$, $k_0=2\pi/L=2\pi$, $k_1=2k_0$, $k_2=3k_0$, and $L\lambda_D^{-1}$ equals, respectively, 0, 0.1, 0.15, and 0.2 in Figs. 2(a)–2(d). These figures show the real part of the Fourier component of the electron density at the wave number $k_{\rm echo}=k_2-k_1$.

The echo amplitude is found to be maximum for noninteracting particles. When $\lambda_D<\infty$ an oscillatory behavior appears, due of course to the plasma collective effects. At the same time, the amplitude decreases, and for $L\lambda_D^{-1}=0.2$ ($k_1\lambda_D=0.628$) the echo has virtually disappeared. Our numerical results thus prove that collective interactions can effectively destroy the echo. This phenomenon was partly recognized by Coste and Peyraud [14], although their complicated analytical treatment could not give a qualitative picture of this phenomenon. Of course, collisional effects or

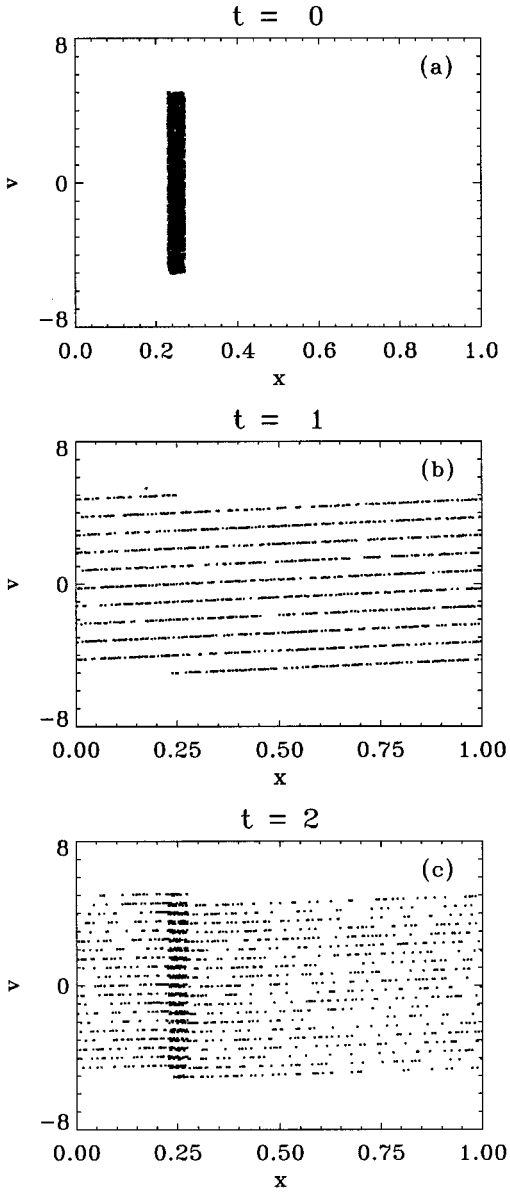

FIG. 3. Phase space representation of 2000 particles (a) at $t=0$; (b) after filamentation has occurred and before the application of the pulse at $t=T^-$; (c) at the time of the echo $t=2T$. Space, time, and velocity are expressed, respectively, in units of L, T, and L/T.

any other truly irreversible phenomena are also very efficient in preventing the formation of the echo, inasmuch as they erase the small scale correlations of the distribution function. This point has been addressed in the original paper by O'Neil and Gould [3] for the case of Coulomb collisions: their estimate is that Coulomb collisions are important when $\nu_{90}\omega_p^2\tau^3>1$, where ν_{90} is the collision frequency at 90 degrees. Some numerical simulations illustrating the effect of a truly irreversible term will be presented in the next section.

III. PARTICLE FOCUSING

Having proven that the echo is mainly due to ballistic motion, we now completely disregard the self-consistent fields. In this case, the particle trajectories can be integrated

exactly, and a Lagrangian code is more convenient. Furthermore, we want to investigate the evolution of an initial condition where all particles are concentrated in a small region compared to the total length L of the domain. More precisely the particles are randomly distributed over a rectangle $x_1<x<x_2$, $-V_m<V<V_m$, with $x_1=L/4$, $x_2-x_1=0.04L$, $V_m=5LT^{-1}$ (the unit of time T is defined below). The boundary conditions in x are again periodic. Contrary to our previous experiments, we do not apply a pulse at $t=0$. In fact, the purpose of this first pulse was to initially create an inhomogeneity in the density, which is now already built in the δ-like initial condition. After a time T, we apply a sinusoidal pulse of the form $\varepsilon \sin(2\pi mx/L)$, where ε is the velocity modulation. The evolution of $N_p=2000$ particles is illustrated in Fig. 3: it is seen that at $t=2T$ the initial state is partially reconstructed. By counting the number of particles that fall again in the region $x_1<x<x_2$, we find it to be roughly 35% of the total number of particles, while a uniform distribution (which would be expected when filamentation in phase space has occurred) would give of course $(x_2-x_1)/L=4\%$. Note that, in this group of simulations, we normalize time to T and length to L, and all figure axes are expressed in normalized units. In this particular case the amplitude and wave number of the perturbation are $\varepsilon=0.175LT^{-1}$ and $m=2$.

If the particles are initially located around x_i (with a small dispersion $\Delta x_i \ll L$), we have found ''empirically'' that the final position x_f is given by the formula (for $m=2$)

$$x_f=-x_i+L/2. \tag{5}$$

This expression is invariant when x_i and x_f are interchanged. We have found that the echo amplitude is maximum when $x_i=x_f\equiv x_0$, which gives $x_0=L/4$. This was the choice of the previous example.

In order to give a theoretical basis to the ''empirical'' formula (5), we adopt the same Lagrangian approach of O'Neil and Gould [3]. The trajectory of a single particle with initial conditions (x_0,v_0) is given by the following expression, valid for $t>T$:

$$x(t,x_0,v_0)=x_0+tv_0+\varepsilon(t-T)\sin[k_m(x+v_0T)], \tag{6}$$

where $k_m=2\pi m/L$. Liouville's theorem states that the distribution function f and the volume element $dxdv$ are both conserved along a trajectory. Consequently

$$f(x,v,t)dx\,dv=f(x_0,v_0,0)dx_0dv_0.$$

Now, assuming the initial distribution to be $f(x_0,v_0,0)=g(v_0)\delta(x_0-x_i)$, we can calculate the nth component of the Fourier transform of the spatial density at time t:

$$\rho_n=\frac{1}{L}\int\int f(x,v,t)\exp(-ik_nx)dx\,dv.$$

With the help of Liouville's theorem, we obtain

$$\begin{aligned}\rho_n&=\frac{1}{L}\int\int f(x_0,v_0,0)\exp[-ik_nx(t,x_0,v_0)]dx_0dv_0\\&=\frac{1}{L}\sum_{s=-\infty}^{\infty}(-1)^sJ_s[k_n\varepsilon(t-T)]\exp[-i(k_n-sk_m)x_i]\\&\quad\times\int dv_0g(v_0)\exp[-iv_0(tk_n-Tsk_m)].\end{aligned} \tag{7}$$

In deriving Eq. (7) we have made use of the identity

$$\exp(-i\alpha\sin\theta)=\sum_{s=-\infty}^{\infty}(-1)^sJ_s(\alpha)\exp(is\theta),$$

where the J_s are Bessel functions of the first kind.

If the support of the function $g(v)$ in velocity space is much larger than LT^{-1}, the last integral in Eq. (7) can be well approximated by a δ function $\delta(nt-msT)$. Since s must be an integer number, the time t must satisfy

$$q\equiv\frac{t}{T}\frac{n}{m}=\text{integer}. \tag{8}$$

By performing the sum in Eq. (7), and remembering that $(-1)^s=\exp(\pm i\pi s)$, we obtain the following result:

$$\rho_n=\frac{1}{L}J_q[k_n\varepsilon(t-T)]\exp\left\{-ik_n\left[\left(1-\frac{t}{T}\right)x_i\pm\frac{t}{T}\frac{L}{2m}\right]\right\}. \tag{9}$$

If we replaced the Bessel function J_q with a constant, Eq. (9) would be the Fourier transform of a δ function centered at the point

$$x_f=\left(1-\frac{t}{T}\right)x_i\pm\frac{t}{T}\frac{L}{2m}. \tag{10}$$

Substituting the parameters of our previous simulations, i.e., $t=2T$ and $m=2$, Eq. (10) turns out to be identical to Eq. (5) [in this case, the second term on the right-hand side of Eq. (10) becomes $\pm L/2$, and, because of periodicity, both signs give the same contribution]. Of course, with different values of t and m, it is possible to recover a greater variety of echoes, but, for the sake of simplicity, we focus our study on the case $t=2T$ and $m=2$.

It is clear that, for the relation (10) to be approximately true, the Bessel function $J_q[k_n\varepsilon(t-T)]$ must be a slowly decreasing function of n, since in this case the Fourier transform of ρ_n is highly peaked around x_f. In order to investigate this point, we need to study the behavior of the function $J_n(Cn)$ for $n\gg1$ [15]. It turns out that three asymptotic expressions hold, respectively, for $0<C<1$, $C>1$, and $C=1$:

$$J_n(n\,\mathrm{sech}\alpha)=\frac{\exp[n(\tanh\alpha-\alpha)]}{\sqrt{2\pi n\tanh\alpha}}\quad(\alpha>0), \tag{11a}$$

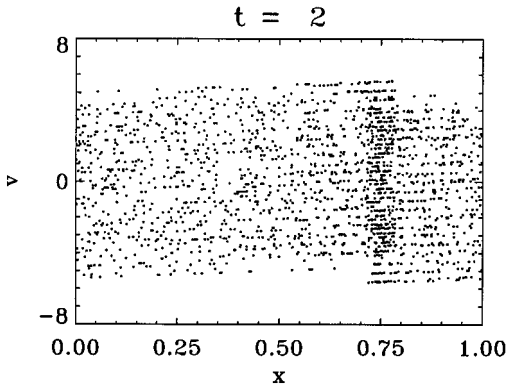

FIG. 4. Phase space representation at $t=2T$ for the case $\varepsilon=0.75LT^{-1}$. The echo appears at $x_f\simeq 0.75L$, as predicted by the theory. Space, time, and velocity are expressed, respectively, in units of L, T, and L/T.

$$J_n(n\sec\beta)=\sqrt{2/(\pi n\tan\beta)}\cos\left(n\tan\beta-n\beta-\frac{\pi}{4}\right)$$

$$\left(0<\beta<\frac{\pi}{2}\right), \quad (11b)$$

$$J_n(n)\propto n^{-1/3}. \quad (11c)$$

Restricting ourselves to the case of our previous simulation, the Bessel function we have to consider is $J_n(k_n\varepsilon T)$, and therefore $C=2\pi\varepsilon TL^{-1}$. When $0<C\ll 1$, Eq. (11a) applies and $\alpha\gg 1$: the Fourier coefficient ρ_n therefore falls rapidly (exponentially) with n, and the particle density $\rho(x)$ will cover almost uniformly the interval $[0,L]$. This is natural, since the echo must disappear for $\varepsilon\to 0$. For α approaching zero, the exponential in Eq. (11a) becomes almost constant and the $n^{-1/2}$ dependence dominates: this results in more and more particles accumulating at x_f at the time $t=2T$. The value $\alpha=0$ (corresponding to $C=1$) is singular, and in this case Eq. (11c) applies. The maximum echo amplitude is to be expected nearby the value $C=1$, since the $n^{-1/3}$ dependence is the slowest one compatible with the expressions (11). In our variables this means $\varepsilon=L/2\pi T$, and, with the units adopted in the simulation ($L=T=1$), $\varepsilon=1/2\pi\approx 0.16$, very close to the value $\varepsilon=0.175$, which was found ''empirically'' by computer experiments.

When $C>1$, Eq. (11b) applies, and the Fourier coefficient ρ_n behaves like $n^{-1/2}$, its dispersion in n decreasing with increasing $C=\sec\beta$, so that for $C\to\infty$ the density $\rho(x)$ again becomes uniform. Furthermore, the cosine in Eq. (11b) should split the echo in two, and shift its position of a quantity $\Delta x_f=\pm(\tan\beta-\beta)L/2\pi$, where $\sec\beta=2\pi\varepsilon TL^{-1}$. This point has been verified by numerical simulations taking a value of $\varepsilon=0.75$ such as $\Delta x_f\simeq\pm L/2$. In this case, the two parts of the echo will recombine at $x_f'=x_f+L/2\simeq 0.75L$ (Fig. 4). This last point could not be guessed on simple grounds, and reassures us of the correctness of our theory.

The amplitude A of the echo can be estimated more precisely. We integrate the density, Eq. (9), in the vicinity of x_f over an interval of width equal to 2Δ:

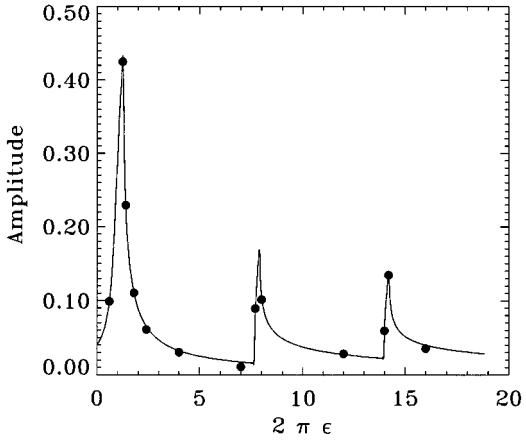

FIG. 5. Amplitude of the echo as a function of the velocity modulation $2\pi\varepsilon$. The solid curve is computed from the theoretical result Eq. (12) in the case $m=2,t=2T$. The dots are results from computer experiments. Space, time, and velocity are expressed, respectively, in units of L, T, and L/T.

$$A\equiv\int_{x_f-\Delta}^{x_f+\Delta}\rho(x)dx=\frac{2\Delta}{L}+\sum_{n=1}^{\infty}J_q[k_n\varepsilon(t-T)]\frac{4}{k_nL}\sin(k_n\Delta), \quad (12)$$

where q is given by Eq. (8). In deriving Eq. (12), use has been made of Eqs. (8)–(10), and of the relation $J_{-n}(-x)=J_n(x)$, and the mode $n=0$ has been treated separately. Note that the first term of this series gives the fraction of particles to be expected in the interval $[x_f-\Delta,x_f+\Delta]$ in the case of a uniform density, i.e., $2\Delta/L$. The series of Eq. (12) is convergent and its sum can be computed numerically. In order to compare with a computer experiment, we have performed a simulation with $m=2,t=2T,2\pi\varepsilon=1.25LT^{-1}$, with zero spatial dispersion in the initial condition (all particles are initially located at $x_i=0.25L=x_f$) and a larger dispersion in velocity space ($V_m=19LT^{-1}$). We obtain $A=0.436$ for the computer experiment, and $A=0.431$ by summing the series of Eq. (12). The small error comes from the finite number of particles used and from the finite dispersion of the initial condition in velocity space. The function $A(2\pi\varepsilon)$ is plotted in Fig. 5 and displays a number of relative maxima. The first one is located at $2\pi\varepsilon\simeq 1$. The other maxima are located at points for which $\tan\beta-\beta=2\pi p$, for $p=1,2,3,\ldots$, and $\sec\beta=2\pi\varepsilon$, according to Eq. (11b). At these values of ε, the cosine in Eq. (11b) shifts the echo position of a multiple of the box length L. The theoretical curve of Fig. 5 has been checked against various computer experiments, with good agreement between the two.

When most of the particles have focused around $x_i=x_f$ at the time $t=2T$, the system is in a state similar to its initial condition. Thus, if we let it evolve, and then apply another pulse at $t=3T$, a new focusing will take place at $t=4T$. Generally speaking, if we apply a pulse at $t=(2l-1)T$, for $l=1,2,3,\ldots$, the particles will focus around x_f for all times $t=2lT$. Computer experiments confirm this behavior: the number of particles falling in the initial region around $x_i=0.25L$ [shown in Fig. 6(a)] strongly peaks at $t=2lT$. More interestingly, there is no sign of decaying and, after a

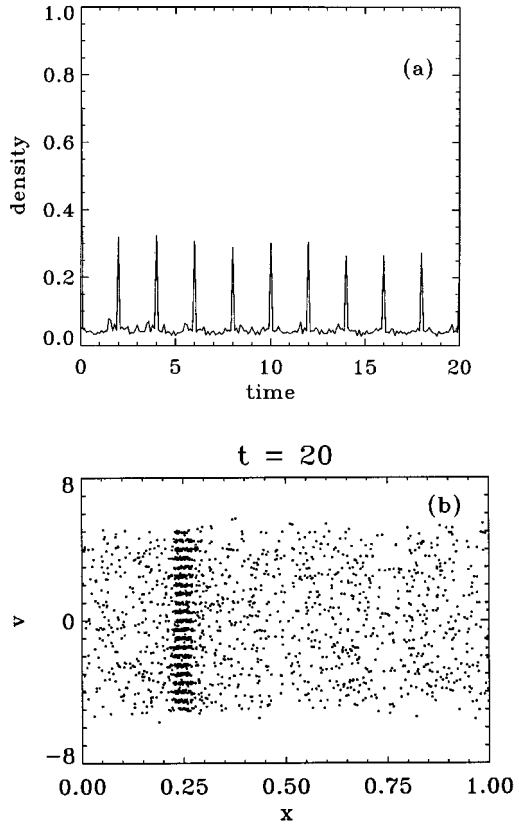

FIG. 6. (a) Fraction of the particles with position in the initial interval $x_1<x<x_2$ as a function of time. A pulse is applied at $t=T,3T,5T,\ldots$. The density peaks at times $t=2T,4T,6T,\ldots$. (b) Phase space representation at $t=20T$. The periodic pulses suppress filamentation and the echo is still clearly visible after ten pulses. Space, time, and velocity are expressed respectively in units of L, T, and L/T.

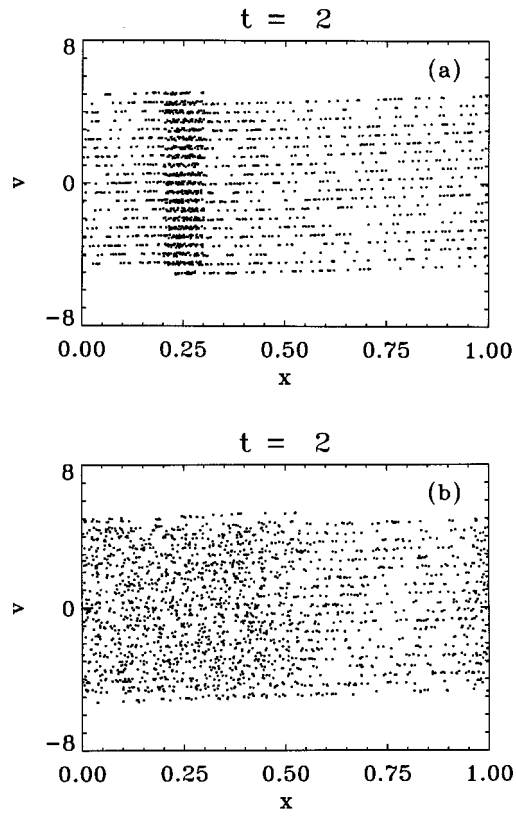

FIG. 7. Phase space representation of 2000 particles for the same case of Fig. 3. Now the particle velocity has been modified of a random quantity $\delta\varepsilon$ at $t=T$. (a) $\delta\varepsilon_{\max}=0.3\varepsilon$;(b) $\delta\varepsilon_{\max}=3\varepsilon$. Space, time, and velocity are expressed, respectively, in units of L, T, and L/T.

large number of pulses, peaks of 30% are still observed. At $t=20T$ (after ten pulses) the echo is still clearly visible [Fig. 6(b)]. This result is surprising, since one would expect a smaller and smaller fraction of the particles participating in the echo. It proves that the background particles, although spread over the entire box in an apparently random way, still keep memory of their initial condition.

Now, we note that our previous prescription defines a well-known Hamiltonian dynamical system, the ''periodically kicked rotor'' [16] with a period $\tau=2T$. The equations of motion for the kicked rotor are

$$\frac{dx}{dt}=v; \quad \frac{dv}{dt}=\varepsilon\sum_{l=1}^{\infty}\delta(t-l\tau)\sin(2\pi mx/L).$$

It is also known that such a system becomes chaotic when $\varepsilon\tau mL^{-1}>c$, where ε is the velocity modulation due to the pulse, and c is a number of order unity. When this inequality is satisfied, the particles diffuse in velocity space with a diffusion coefficient $D\simeq m^2\varepsilon^2\tau^{-1}$. Our simulations have proven that the echo amplitudes reaches its maximum value when $\varepsilon\tau mL^{-1}\simeq c$, i.e., at the borderline with the chaotic regime. Therefore, we have shown the existence, for a very simple dynamical system, of an intermediate regime between the integrable and the chaotic ones. In the integrable regime ($\varepsilon\tau mL^{-1}\ll 1$) the trajectories are periodic and each particle keeps an approximately invariant velocity: all spatial inhomogeneities in the initial condition are damped away by phase mixing. In the chaotic regime ($\varepsilon\tau mL^{-1}\gg 1$), the particles experience a ''random'' sequence of kicks, each one either increasing or reducing its velocity, which results in a random walk in velocity space. The intermediate regime ($\varepsilon\tau mL^{-1}\simeq 1$) corresponds to a resonance condition, when the velocity pulse ε approximately equals the distance between two filaments in velocity space after at time τ (which is of the order $L/m\tau$). When this condition is satisfied, the system responds to the external excitation by resonantly oscillating at the same frequency τ^{-1}, but with a dephasing of half a cycle. This response is seen as an ''echo'' bringing back a large number of particles to their initial positions at $t=\tau,2\tau,3\tau,\ldots$.

Finally, we briefly investigate the effect of introducing a truly irreversible term in our original equations (we remind the reader that all dynamics treated so far are time reversal invariant). In order to do so, we slightly perturb the particle velocities right after the sinusoidal pulse at $t=T$. The perturbation $\delta\varepsilon$ is a random number uniformly distributed in the interval $[-\delta\varepsilon_{\max},\delta\varepsilon_{\max}]$. We expect the echo to disappear when $\delta\varepsilon_{\max}\simeq\varepsilon$, since this would destroy the correlations hidden in velocity space. The numerical results confirm this conjecture (Fig. 7): the echo is still quite visible for $\delta\varepsilon_{\max}=0.3\varepsilon$, but has virtually disappeared when $\delta\varepsilon_{\max}=3\varepsilon$.

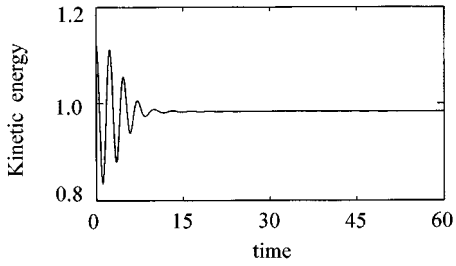

FIG. 8. Dynamics of noninteracting particles in an anharmonic potential: time evolution of the kinetic energy in the classical case ($H=0$). Arbitrary units.

IV. LINEAR QUANTUM ECHO

In order to evaluate the quantum corrections to classical dynamics, it is useful to adopt the Wigner representation [7–10], according to which quantum mechanics can be expressed in a phase space formalism. The quantum distribution function $W(x,p,t)$ has all the good properties of its classical counterpart, except positivity. The evolution of W is given by the Wigner equation, which replaces the classical Liouville equation

$$\frac{\partial W}{\partial t}+\frac{p}{m}\frac{\partial W}{\partial x}=\frac{i}{2\pi\hbar^2}\int\int\left[\phi\left(x-\frac{z}{2},t\right)-\phi\left(x+\frac{z}{2},t\right)\right]\times\exp\left(-\frac{i}{\hbar}(p-p')z\right)W(x,p',t)dzdp', \tag{13}$$

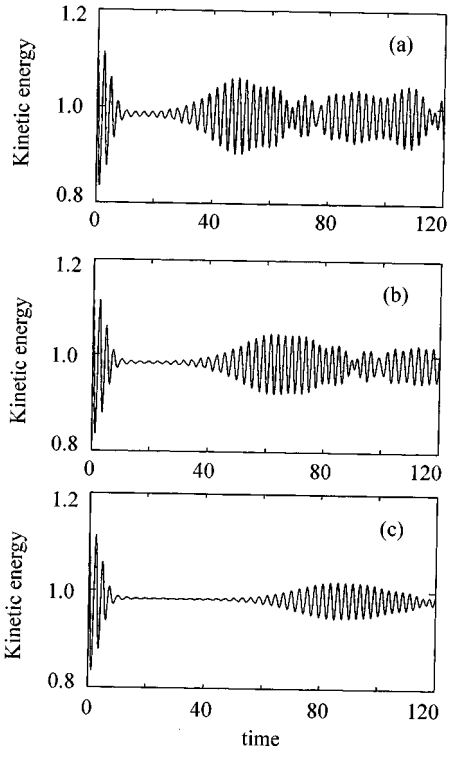

FIG. 9. Same as Fig. 8 in the quantum case. (a) $H=0.16$; (b) $H=0.12$; (c) $H=0.08$. Arbitrary units.

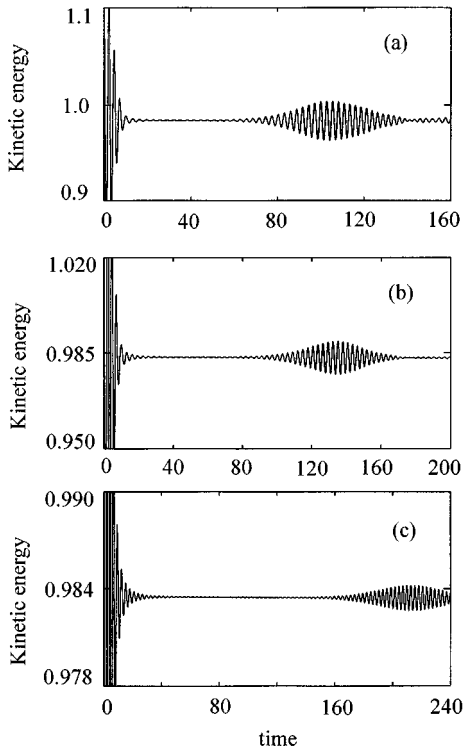

FIG. 10. Same as Fig. 8 with (a) $H=0.06$; (b) $H=0.04$; (c) $H=0.02$. Arbitrary units.

where $\phi(x,t)$ is the potential.

We make use of the Wigner equation to show that quantum mechanics allows for the appearance of linear echoes. Evidence of this phenomenon has already been pointed out in the literature [17–21]; our work attempts, however, to solve the Wigner equation directly, while many previous studies focused on the numerical solution of the Schrödinger equation. This is an important point for a number of reasons. (1) The Wigner representation enables us to work with the most general class of quantum mechanical mixed states, whereas only pure states can be represented by a Schrödinger wave function. (2) Phase mixing and echoes are statistical concepts (involving a large number of particles), and therefore classical mechanics should be compared to *statistical* quantum mechanics, rather than to single particle quantum mechanics. (3) The approach to the classical limit is a very delicate operation in the Schrödinger formalism (a semiclassical state is represented by a strongly oscillating wave function), whereas it is very natural in the Wigner formalism (one just lets $\hbar$ go to zero): it is thus possible to compare the evolution of exactly the same initial condition for different values of Planck's constant. (4) Finally, the phase space picture allows for a direct visual comparison between classical and quantum results. In particular, it will be clear from our simulations that quantum effects prevent complete phase mixing, which is the ultimate reason for the appearance of the echo.

We now turn to the numerical simulation of the dynamics of noninteracting particles in a confining potential. The simplest choice would be the harmonic oscillator, but it can be shown easily that the dynamics of the harmonic oscillator has no quantum corrections in the Wigner representation

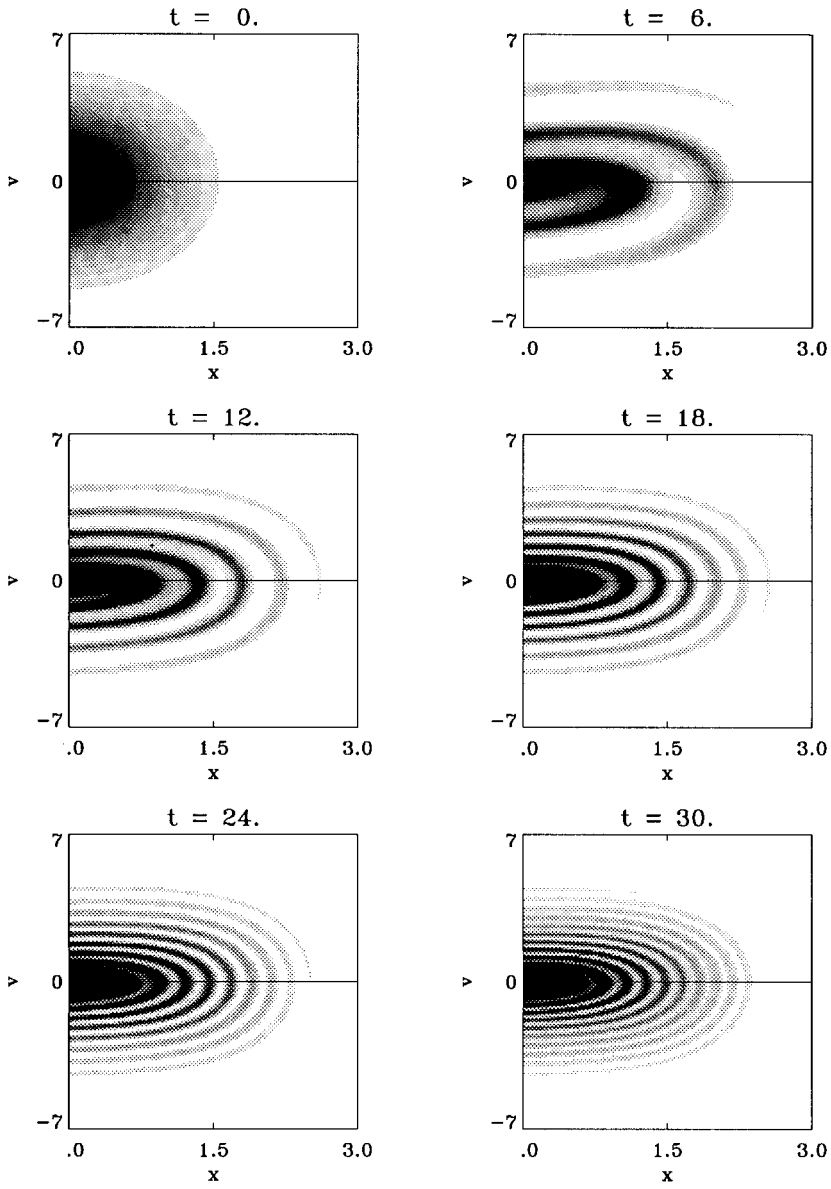

FIG. 11. Classical phase space for the anharmonic oscillator. For negative x, the figures are symmetric with respect to the origin of axes. Arbitrary units.

[22]. Therefore, we introduce an anharmonic term [23,24], and consider the following quartic potential:

$$\phi(x)=\tfrac{1}{2}m\omega^2x^2+\tfrac{1}{4}m\beta x^4. \tag{14}$$

By injecting this potential in Eq. (13), one can easily verify that the Wigner equation takes the following form:

$$\frac{\partial W}{\partial t}+\frac{p}{m}\frac{\partial W}{\partial x}-m(\omega^2x+\beta x^3)\frac{\partial W}{\partial p}=-\frac{\hbar^2m\beta}{4}x\frac{\partial^3W}{\partial p^3}. \tag{15}$$

Note that only the first quantum correction (in $\hbar^2$) has survived, and this correction disappears for $\beta=0$ (purely harmonic potential). The relative importance of quantum effects is conveniently measured by the dimensionless parameter $H=\hbar\beta/m\omega^3$. We have solved the Wigner equation with a Gaussian initial condition centered at $x=p=0$, with dispersions $\sigma_x=1$, $\sigma_p=1.5$ such as $\sigma_x\sigma_p>\hbar/2$ to ensure Heisenberg's uncertainly principle. Other parameters in the definition of the potential are $\omega=m=1,\beta=0.2$. In Fig. 8 we have plotted the evolution of kinetic energy against time. In the classical case ($H=0$), the kinetic energy relaxes to a stationary value: this is due to the phase mixing induced by the quartic term in the potential.

When H is small, but not zero, the kinetic energy also relaxes to the same value, but, at a subsequent time, an oscillation (the echo) appears. The evolution of the kinetic energy is represented in Figs. 9 and 10 for different values of H. When H decreases, the echo amplitude goes to zero, while the time of its appearance is rejected to infinity. From these and other simulations, we have tried to estimate how the echo time varies as a function of H. If one takes for t_{echo} the time of maximum echo amplitude, a rough estimate gives $T_{\text{echo}}\simeq H^{-\mu}$ with $1/2<\mu<2/3$. This result rules out such laws as H^{-1} or $\log H^{-1}$, the former being too fast and the latter too slow. The log dependence has bee proposed as a typical time of validity of the semiclassical approximation for chaotic dynamical systems [25]: since our Hamiltonian is integrable, it is not surprising that the classical behavior lasts for a longer time.

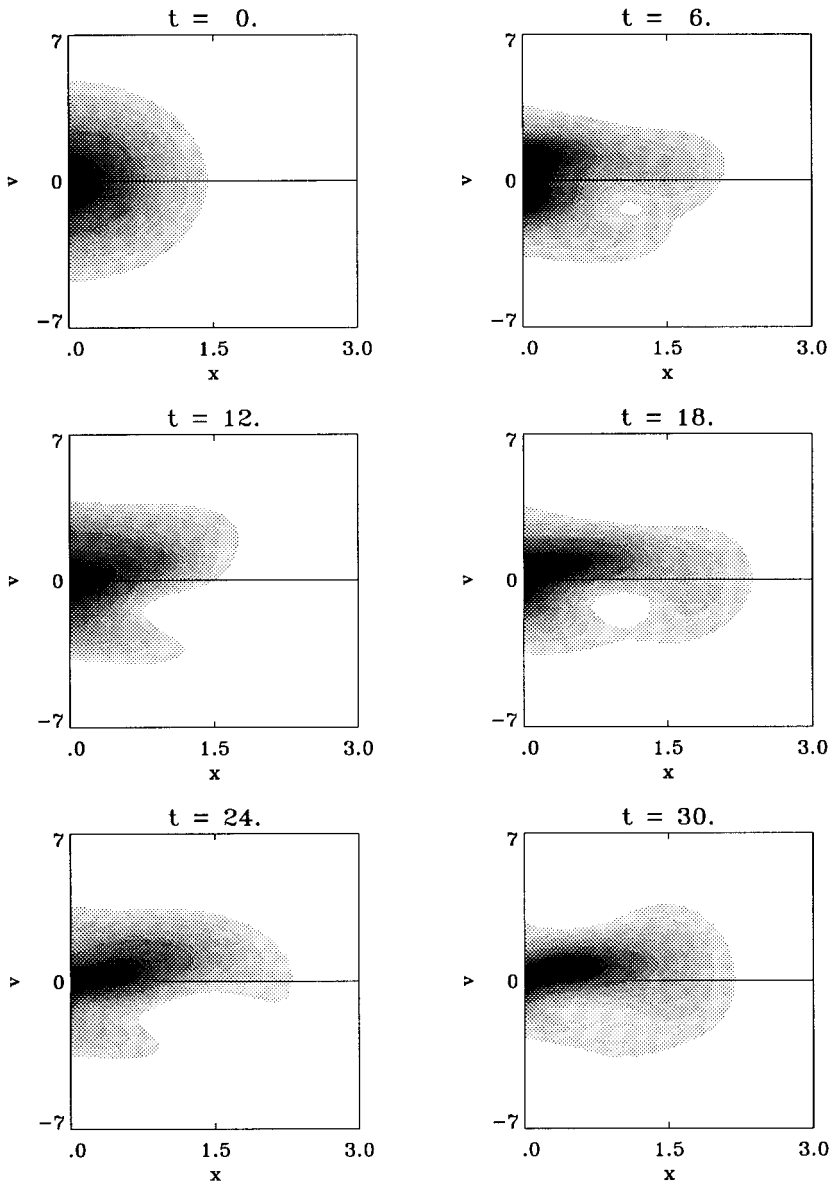

FIG. 12. Quantum phase space for the same case of Fig. 11, with $H=1.2$. Positive part of the Wigner function. Arbitrary units.

Figure 11 shows, in the classical case, the phase portrait for the evolution of a Gaussian initial state ($\sigma_x=0.6$, $\sigma_p=2$) in the quartic potential described by Eq. (15), with $\omega=m=1, \beta=0.8$. The distribution function soon develops a spiral structure, displaying a very fine filamentation, which is the ultimate cause of the kinetic energy relaxation. The same simulation is repeated in the quantum case ($H=1.2$). Figure 12 shows the positive part of the Wigner function, and Fig. 13 its negative part (the respective maxima are in a ratio of about 20). We see that complete phase mixing is stopped by a nonzero Planck constant, via the formation of negative islands in the distribution function. The correlations among these structures are responsible for the appearance of the echo.

According to Fig. 8, the classical kinetic energy relaxes to a constant value, and no echo is ever observed. Physically, as we have seen, this is due to phase space filamentation. This behavior might seem in contrast with the results of Sec. III, in which a classical dynamical system displayed a variety of echo phenomena. There is, however, an important difference: in the case of the quartic oscillator, the initial state is left to evolve without any other external intervention. On the contrary, for the case of Sec. III, a sinusoidal pulse is applied at $t=T$: it is precisely this intervention that allows for the appearance of the echo. Otherwise, in the absence of such a pulse, the corresponding distribution function would filament, just as in the case of the oscillator. It is, however, remarkable that a simple macroscopic operation, such as applying a sinusoidal pulse, can induce a partial reconstruction of the initial condition.

It is also interesting to note the different properties of the classical and quantum phase space as far as reversibility is concerned. According to Lebowitz [1], the main signature of irreversible dynamics is the possibility of ordering a sequence of snap-shots of the physical system with increasing time. Thus, in the case of two miscible liquids of different colors (say, ink and water), a picture showing a localized drop of ink in otherwise colorless water must precede (and indeed does in the real world) another picture representing a liquid of roughly uniform color. In the same way, the sequence of Fig. 11 for the classical phase space can easily be ordered with time: the more filaments are present, the

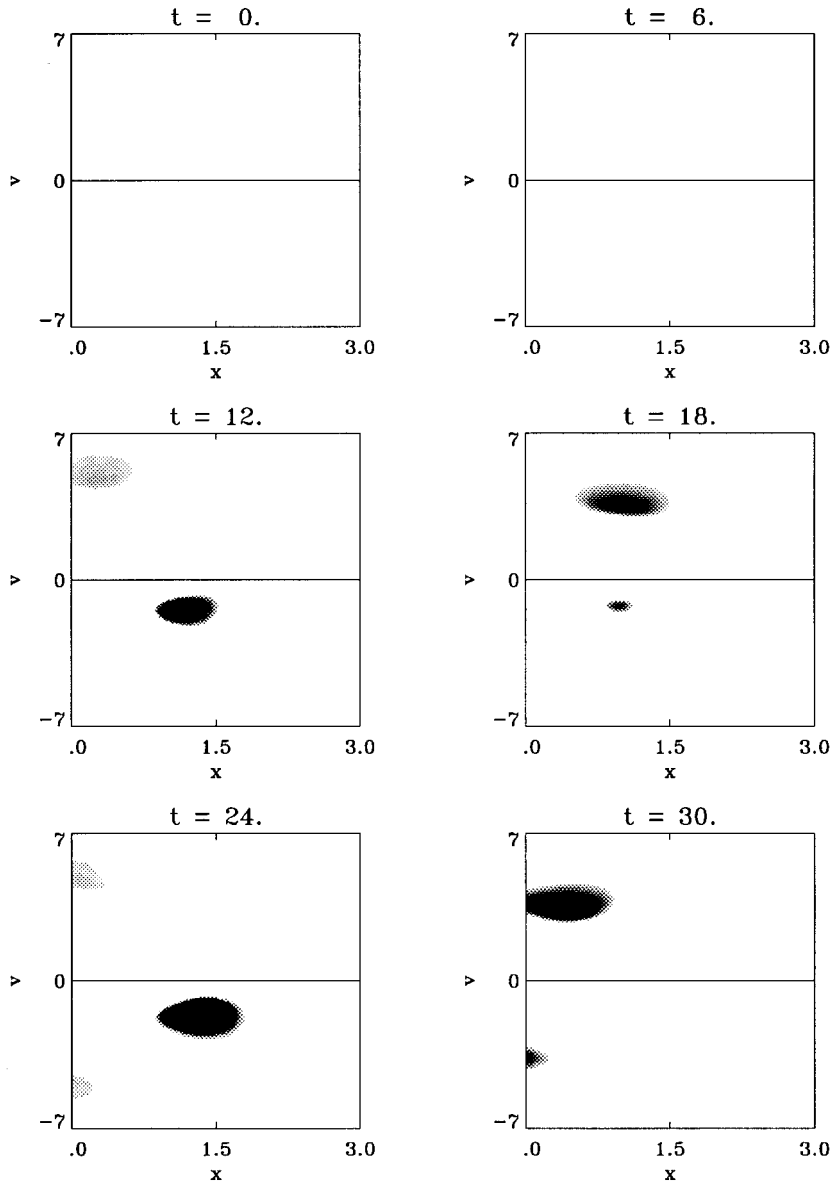

FIG. 13. Same as Fig. 12: the negative part of the Wigner function is shown here. The maximum of the positive part of the Wigner function is approximately 20 times larger than the maximum of the negative part. Arbitrary units.

''older'' the picture. This is therefore a case of irreversible dynamics, as illustrated by the relaxation of the total, macroscopic kinetic energy (Fig. 8) (incidentally, this is so even if our dynamical system is integrable: irreversibility is a separate issue from integrability and chaos, as pointed out by Lebowitz [1]). The reader might be surprised that a simple, anharmonic oscillator turns out to be an irreversible system if we accept the above definition of irreversibility (which is a very plausible and easily testable one). To dissipate any possible confusion, we stress that the macroscopic physical system that we are considering is *not* a single oscillator, but rather a collection of an infinite number of independent oscillators. Each individual oscillator represents one of the microscopic constituents forming our macroscopic system, which is described by Eq. (15) with $\hbar=0$, i.e., by Liouville's equation. Note that we are just rephasing the textbook definition of a statistical ensemble, only from a more ''realistic'' point of view: for us, each element of the ensemble is not a convenient fiction, but a real constituent of some macroscopic physical object. For an observer who can only measure macroscopic quantities (such as the total kinetic energy plotted in Fig. 8), the system will effectively behave in an irreversible way: the kinetic energy oscillates and then decays to a constant value, but the opposite (oscillations arising spontaneously) never occurs. Of course, the fact that this system is integrable has an impact on the dynamics. Since the oscillators are independent and each of them preserves its energy, the accessible region of phase space is greatly reduced. For example, if the initial distribution occupies an annulus of energy $E_1<E<E_2$, points outside this region are not of course accessible. However filamentation still occurs, and the total kinetic energy will still relax as in Fig. 8.

On the other hand, for the quantum phase space (Figs. 12 and 13), there is no self-evident way of arranging the pictures with increasing time, and therefore no irreversible behavior. Heuristically, this can be understood by the following argument. If we define a microscopic constituent as a region in phase space of volume $\hbar$, the classical, macroscopic system contains an infinite number of microscopic constituents (the individual oscillators referred to in the previous paragraph). On the contrary, the number of microscopic constituents contained in the quantum system is finite, and propor-

tional to $\sigma_p \sigma_x / \hbar$. When this ratio is not large, some reversible behavior is to be expected. In this case, in fact, the first of the conditions for irreversibility mentioned in Sec. I has been violated. The onset of irreversibility is thus, at least in this case, closely related to the relative importance of quantum effects.

V. CONCLUSION

In this paper we have investigated the properties of a few dynamical systems that are invariant with respect to time reversal, and nevertheless display an effective irreversible behavior for suitable macroscopic quantities. Plasma wave echoes are particularly interesting in this respect, since they represent a nice example of partial reversibility, which is triggered by a simple macroscopic operation (an instantaneous sinusoidal velocity modulation). This kind of macroscopic reversibility is, in our opinion, more interesting than the microscopic reversibility due to velocity reversal. We have shown that not only collisional damping, but also collisionless self-consistent interactions can effectively reduce the amplitude of the echo. The echo is therefore a typically ballistic effect: to prove this, we have performed a series of computer experiments in which we progressively switch on collective effects by increasing the particle charge.

When the initial condition is highly inhomogeneous (''δ-like''), only one pulse is needed to obtain a variety of echo phenomena. By periodically repeating the pulse, one can focus a considerable fraction of the particles in a small spatial region, without any appreciable losses for very long times. This is an effective way of suppressing phase mixing by means of a macroscopic operation. This regime is situated in between the integrable and the chaotic regimes of the periodically kicked rotor.

Quantum echoes have been investigated in the case of an anharmonic potential by making use of the Wigner formalism, which expresses quantum mechanics in the familiar phase space representation. It was found that quantum mechanical effects prevent complete phase mixing, and consequently allow for the appearance of a linear echo. The results obtained have been interpreted in terms of the reversibility properties of our physical system. In particular, we have stressed that irreversibility arises (1) because the number of microscopic constituents (i.e., degrees of freedom) contained in a macroscopic object is extremely large, and (2) because an observer can only measure macroscopic quantities. Our physical object (an infinite collection of anharmonic oscillators) has an integrable dynamics, nevertheless it behaves irreversibly as far as macroscopic observables are concerned. When quantum effects are taken into account, the first of these conditions may not be satisfied, and a reversible behavior is observed.

We have performed a more extensive investigation of the reversibility properties of classical and quantum systems in a previous publication [10], to which we refer the interested reader. It is our feeling that this point deserves further investigations, and could shed new light on the subtle problem of the semiclassical limit.

[1] J. L. Lebowitz, Phys. Today **46** (9), 32 (1993).
[2] E. L. Hahn, Phys. Rev. **80**, 580 (1950); S. Zhang, B. H. Meier, and R. R. Ernst, Phys. Rev. Lett. **69**, 2149 (1992).
[3] T. M. O'Neil and R. W. Gould, Phys. Fluids **11**, 134 (1968).
[4] D. R. Baker, N. R. Ahern, and A. Y. Wong, Phys. Rev. Lett. **20**, 318 (1968); A. Y. Wong and D. R. Baker, Phys. Rev. **188**, 326 (1969).
[5] C. Z. Cheng and G. Knorr, J. Comput. Phys. **22**, 330 (1976).
[6] A. Ghizzo, P. Bertrand, M. M. Shoucri, T. W. Johnston, E. Fijalkow, and M. R. Feix, J. Comput. Phys. **90**, 431 (1990).
[7] E. P. Wigner, Phys. Rev. **40**, 749 (1932).
[8] V. I. Tatarskii, Usp. Fiz. Nauk **139**, 587 (1983) [Sov. Phys. Usp. **26**, 311 (1983)].
[9] N. D. Suh, M. R. Feix, and P. Bertrand, J. Comput. Phys. **94**, 403 (1991).
[10] G. Manfredi and M. R. Feix, in *Advances in Kinetic Theory and Computation*, edited by B. Perthame (World Scientific, Singapore, 1994), pp. 109–140.
[11] F. F. Chen, *Introduction to Plasma Physics and Controlled Fusion* (Plenum, New York, 1984), Vol. 1.
[12] J. U. Brackbill, Phys. Fluids **15**, 1358 (1972).
[13] J. C. Baker and W. J. B. Oldham, Jr., Phys. Fluids **12**, 1525 (1969).
[14] J. Coste and J. Peyraud, J. Plasma Phys. **3**, 603 (1969).
[15] *Handbook of Mathematical Functions*, edited by M. Abramowitz and I. A. Stegun (Dover, New York, 1965), pp. 365–366.
[16] R. Artuso, G. Casati, and D. Shepelyansky, Phys. Rev. Lett. **68**, 3826 (1992).
[17] P. Kasperkovitz and M. Peev, Phys. Rev. Lett. **75**, 990 (1995).
[18] R. Grobe and F. Haake, Z. Phys. B **68**, 503 (1987).
[19] F. Haake, M. Kus, and R. Scharf, Z. Phys. B **65**, 381 (1987).
[20] S. L. Barnett and P. L. Knight, Phys. Rev. A **33**, 2444 (1986).
[21] R. R. Puri and G. S. Agarwal, Phys. Rev. A **33**, 3610 (1986).
[22] G. Manfredi, S. Mola, and M. R. Feix, Eur. J. Phys. **14**, 101 (1993).
[23] H. J. Korsch and M. V. Berry, Physica D **3**, 627 (1981).
[24] G. J. Milburn, Phys. Rev. A **33**, 674 (1986).
[25] S. Tomsovic and E. J. Heller, Phys. Rev. E **47**, 282 (1993).